ANALYTICAL, FIRST PRINCIPLES MODELING OF ELASTOMERIC DAMPERS

Sesi Kottapalli
Flight Vehicle Research and Technology Division
NASA Ames Research Center
Moffett Field, California
Sesi.B.Kottapalli@nasa.gov

Olivier A. Bauchau
School of Aerospace Engineering
Georgia Institute of Technology
Atlanta, Georgia
olivier.bauchau@ae.gatech.edu

Changkuan Ju, Serkan Ozbay, Yogesh Mehrotra
Materials Technologies Corporation
Monroe, Connecticut
cju@aboutmtc.net
sozbay@aboutmtc.net
ymehrotra@aboutmtc.net

The goal of this ongoing initial study is to model the critical behaviors of rotorcraft elastomeric dampers, i.e. the hyperelastic, viscous, and nonlinear behaviors involving hysteresis loops. On completion, the current model would not require the physical damper to exist *a priori*, and could be used to optimize damper design concepts. An initial, overall validation effort has demonstrated the successful step-by-step sample development of a new finite element damper model and, importantly, its integration with the multibody dynamics analysis DYMORE. Two material models, the Haupt-Sedlan model and the recently proposed Höfer-Lion model, have been analyzed, and the results have been fitted to sample experimental data. Both models gave acceptable results for the storage and loss moduli. Since at present there is a dearth of available appropriate material data for the typical elastomers used in helicopter dampers, a new experimental effort has been initiated by Materials Technologies Corporation (MTC) and Georgia Tech to conduct materials testing and acquire the required material data.

Notation

A	Harmonic strain amplitude
$c_e, c_{e1}, c_{e2}, c_{e3}$	Coefficients defining τ_e
c_p	Coefficients defining τ_p
c_v	Coefficients defining τ_v
$F, F_{ep}, F_{ev}, F_p, F_v$	Deformation gradient tensors corresponding to γ, γ_{ep}, γ_{ev}, γ_p, γ_v
G	Cauchy-Green strain tensor
G', G''	Storage and loss modulus
I_1, I_2, I_3	Invariants of Cauchy-Green strain tensor
k	Ramp strain rate, also stiffness
L	Length of specimen
p	Spherical stress
q	Structural variable
q_s	Steady state of structural variable q
t_{rec}	Recovery time for structural variable q
W	Width of specimen
$\underline{x}$, $\underline{X}$	Coordinates in reference and deformed configuration
γ	Total shear strain
γ_0	Strain step size in relaxation test
γ_{ep}, γ_{ev}	Elastic strain in plastic and viscous branch
γ_p, γ_v	Plastic and viscous strain
Δ	Shear deformation, also displacement
η_p	Plastic constant
η_v	Viscosity
$\xi, \tau_{max}, \tau_{min}, \zeta, \tau_q$	Material constants

Presented at the American Helicopter Society Aeromechanics Specialists' Conference, San Francisco, CA, January 20-22, 2010. *Copyright © 2010 by the American Helicopter Society International, Inc. All rights reserved.*

σ_{ij}	Second Piola-Kirchhoff stress tensor
τ	Total shear stress
τ_e, τ_p, τ_v	Stresses in elastic, plastic and viscous branch
τ_{ij}	Cauchy stress tensor
τ_{ij}^{dev}	Deviatoric Cauchy stress tensor
$\psi_e, \psi_{ep}, \psi_{ev}$	Strain energy functions corresponding to τ_e, τ_p, and τ_v

Höfer-Lion Model

q	Internal variable
z	Intrinsic time scale
$\alpha, \bar{\tau}, d$	Material parameters
τ_0, τ_q, τ_R	Relaxation time
ω, f	Harmonic strain frequency in [rad/sec] and [Hz]

Introduction

In helicopters, the need to stabilize the lightly damped lead-lag motion of the rotor blades necessitates the use of external dampers. Hydraulic dampers are often used, but they have high maintenance costs, and these high operational/lifecycle costs have led to the development and use of elastomeric dampers. Elastomeric dampers feature simpler mechanical design and a lower part count. The design of elastomeric dampers is hampered by a lack of reliable analytical tools that can be used to predict their damping behavior in the presence of the large multi-frequency motions experienced by the rotor blade, and thus the damper. There is a need to develop advanced modeling tools for the analysis and design of elastomeric components as elaborated below.

Elastomers are hyperelastic materials and their energy dissipation is characterized by hysteresis loops that are dependent on the amplitude and the frequency of the damper motion, and the temperature. The complex nonlinear, hyperelastic, and viscous nature of the materials used in elastomeric dampers makes their analytical modeling difficult. Current analytical models often use simplified representations such as linear device models, but these device models require costly and time consuming testing to construct them. Moreover, neither the material characteristics nor the damper geometric configuration are directly modeled in these simplified device models, Refs. 1-9. The state of the art in first-principles modeling of elastomeric dampers is reflected in the approaches of Refs. 10-11. *Although the basic theory is available, the rotorcraft industry has not made use of this available knowledge in comprehensive dynamics analysis codes.* Instead, the rotorcraft analyses are heavily dependent on the lumped-parameter based device models and consequently, the effects of geometric and dissipative nonlinearities on the damper behavior are not properly accounted.

In this initial study, first principles are used to model rotorcraft elastomeric dampers. First-principles models predict the behavior of a device based on a continuum mechanics approach in which the geometric configuration of the various components of the device is modeled using, for example, a finite element approach, and the material behavior is represented by an appropriate set of nonlinear constitutive laws. Such a model would not require the damper to exist *a priori*, and could be used to optimize the design of a damper concept.

Program goal

The overall objective of this ongoing, multi-year effort is to develop a finite element based tool for modeling the response of complex elastomeric components. This finite element tool will be integrated with a finite element-based multibody dynamics analysis code to accurately and reliably simulate the dynamic response of rotorcraft with elastomeric components. This analysis will utilize first principles-based, nonlinear hyper-viscoelastic formulations. The tools developed in this study will be validated using bench and flight test data.

Technical approach

The overall technical approach, with the following three elements, is shown below in Fig. 1:

1) Establishment of constitutive relationships for the material behavior of carbon filled elastomers,
2) Development of a first principles based finite element model for elastomeric dampers; and
3) Integration of these models within a multibody dynamics code for comprehensive rotorcraft analysis.

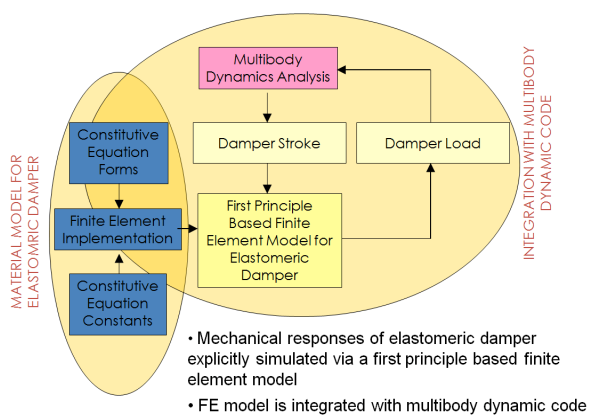

Fig. 1. Overall technical approach.

Overview of current study

This paper is divided into five sections, outlined as follows: first, an Initial Validation study is described in which the basic, overall formulation is validated using simple examples; second, relevant Basics of Elastomer Modeling are given; third, a specific elastomer model of interest, the Haupt-Sedlan model, is described and results using this model are presented; fourth, the recent 2009 Höfer-Lion elastomer model is described and results using this model are presented; and fifth, a completely new experimental effort recently initiated by Materials Technologies Corporation (MTC) and Georgia Tech to obtain material properties is outlined, followed by the Concluding Remarks.

Initial Validation

A nonlinear hyperelastic material formulation, based on the polynomial form of the strain energy density function for the elastomeric material, was implemented. As an example, Fig. 2 below shows a simple damper model consisting of an elastomeric element sandwiched between two aluminum plates. The damper has been modeled as a static, plane strain problem with a thickness of 100 mm. The left edge of the model is fully fixed to the ground. A concentrated load is applied at the lower right corner of the model to simulate damper loads. The model has been analyzed using the currently developed finite element tool (FE tool) as well as the commercially available package ABAQUS. Currently, the multibody dynamics analysis used is DYMORE, Ref. 12. Under the applied load, the strain level in the elastomeric components has been calculated to be ≤ 10%, consistent with the typical strain levels in elastomeric dampers. The discrepancy between the results from the FE tool and the ABAQUS simulations is ≤ 3%.

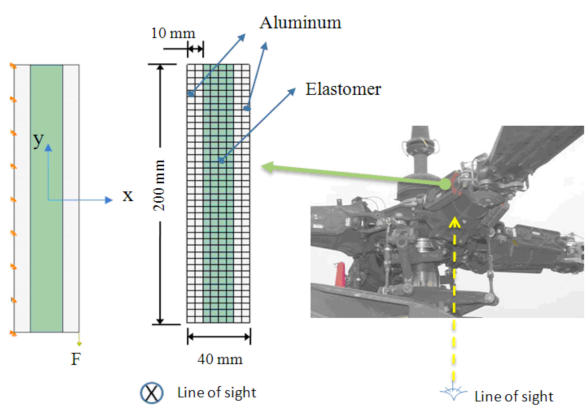

Fig. 2. Simple damper model.

After validating the FE tool for static conditions, the FE tool was modified to include dynamic effects, and dynamic analyses have been performed. A linear strain rate dependent model has been used to represent the viscous properties. Two key results are shown in this, as follows: the dual frequency excitation results and the results that demonstrate the integration of the new finite element tool with the multibody dynamics analysis code DYMORE.

Dual frequency effect

This effect was investigated by calculating the responses of the simple damper model under dual frequency excitation. Typical damper stroke amplitudes at the 1 per/rev and the lag frequency (approximately 0.27 per/rev), respectively, have been prescribed as follows: 7.62 mm and 2.54 mm. The corresponding reaction forces are computed as F_1, F_2 , and F_3. The FE analysis results are shown in Fig. 3 for two different damping coefficients, $\mu = 0.01$ and 0.05 sec. A close look at Fig. 3 verifies that the resulting force F_3 is not a simple superposition of the two forces, F_1 and F_2. These results are as expected since the rule of superposition principle does not apply under nonlinear system conditions. The current first-principles based FE tool captures this behavior as shown by the analysis result $F_3 \neq F_1 + F_2$.

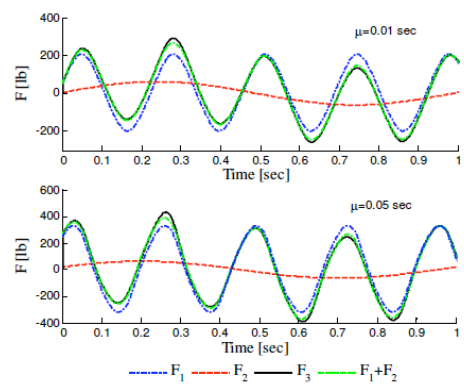

Fig. 3. Dual-frequency excitation. Data show that frequency superposition is not possible due to nonlinearity.

Integration of elastomeric damper with multibody dynamics analysis code

The FE tool was implemented into a multibody dynamics analysis for a complete closed-loop comprehensive analysis of a rotorcraft. A typical dynamic simulation procedure is shown in Fig. 4 below. First, the multibody dynamics analysis code simulates the response of the vehicle based on the current boundary conditions and the information from the previous step. The simulated loadings (displacement) on the damper are used as the boundary conditions for the finite element simulation of the elastomeric damper. The response of the damper (force) is then used for the next simulation step.

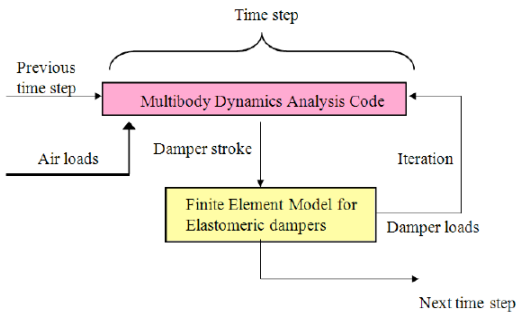

Fig. 4. Integration of present finite element tool with a multibody dynamics analysis code.

In the time domain simulations, a UH-60A rotor at a high-airspeed forward flight condition has been considered using DYMORE. The following two cases have been considered: the elastomeric damper model shown in Fig. 2 and a linear spring-dashpot model. Figure 5 below shows the time histories for the damper stroke and the damper reaction force. It can be seen from the plot on the top that the damper stroking history is almost identical for both models. This is expected as the lead-lag motion is mainly determined by the rotor system. However, as shown in the plot at the bottom, the resulting damper force profiles are distinctly different, since the reaction forces are determined by the respective properties of the dampers.

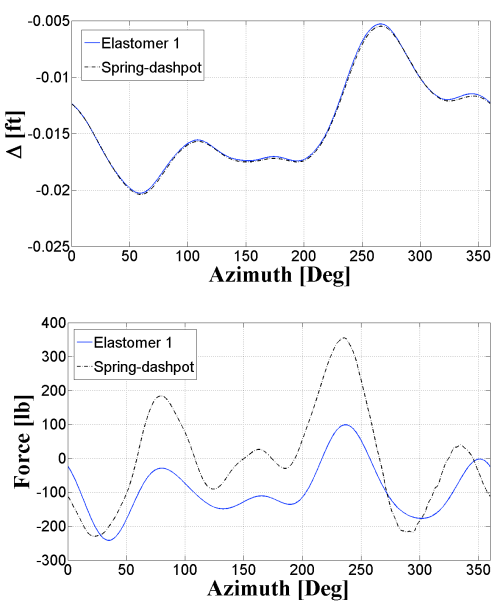

Fig. 5. DYMORE implementation, damper stroke and force comparison for elastomeric and spring-dashpot dampers.

Basics of Elastomer Modeling

To understand the fundamentals of elastomer modeling, a study of the inelastic behavior of such materials is critically important, especially when these materials are used as energy dissipation components, for example, elastomeric dampers. The first inelastic characteristic of elastomeric materials is the nonlinear rate-dependent viscous effect, apparent in relaxation and creep tests. The second inelastic behavior of significance is the amplitude dependence and equilibrium hysteresis effect which is usually modeled by the theory of plasticity. Moreover, the Mullins effect, Refs. 13-14, which is a strain-induced stress-softening during the first few loading cycles is an important inelastic behavior observed in filled elastomers (the Mullins effect is not considered in the current study).

There is no consensus on the most appropriate approach to modeling carbon filled elastomers. At present, it is not clear what phenomena need to be included in the model. Extensive testing is required to determine the material parameters. For some models, many parameters are required. Of the various models available, the internal variables model is commonly used, and can be further classified into the following two main models: deformation decomposition and stress convolution, discussed as follows.

Internal variables based models

One class of the internal variables based models is generalizations of the three-parameter solid models, for instance, the Zener model, Fig. 6. A Zener model consists of a spring and a Maxwell element in parallel. One way to generalize the Zener model is to include more than one Maxwell element in parallel to represent different relaxation times of the material. Another approach is to add plastic elements to the generalized Zener model. These plastic elements model the equilibrium hysteresis effect of the elastomeric materials. The Maxwell and plastic elements are all independent from each other.

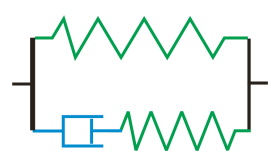

Fig. 6. Zener model.

Internal variables based models: Multiplicative decomposition of deformation gradient: The multiplicative decomposition of the deformation gradient tensor can be explained using a uniaxial rheological model, Fig. 7. This model is a generalization of the Zener model with an additional plastic element. The spring at the top represents the nonlinear elastic behavior. The Maxwell element in the middle models the rate-dependent overstress. Finally, the plastic element at the bottom

describes the rate-independent equilibrium hysteresis effects, Refs. 15-16.

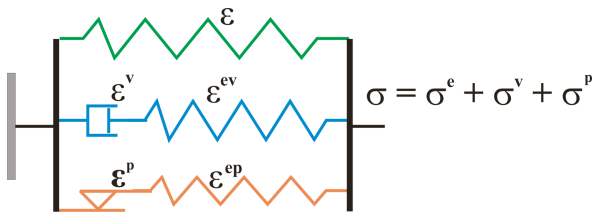

Fig. 7. Uniaxial rheological model.

The stress in each branch is the elastic equilibrium stress σ^e, overstress σ^v, and equilibrium hysteretic stress σ^p, respectively. The total resulting stress is the sum of these three stresses

$$\sigma = \sigma^e + \sigma^v + \sigma^p \tag{1}$$

The total resulting strain, ε, is decomposed into the elastic and viscous parts for the Maxwell element as

$$\varepsilon = \varepsilon^{ev} + \varepsilon^{v} \tag{2}$$

or, into the elastic and plastic strains for the plastic branch as

$$\varepsilon = \varepsilon^{ep} + \varepsilon^{p} \tag{3}$$

The strain energy function is the sum of three strain energy functions, which are related to the three springs in the model, respectively:

$$\psi = \psi_e(\varepsilon) + \psi_{ev}(\varepsilon^{ev}) + \psi_{ep}(\varepsilon^{ep}) \tag{4}$$

In particular, ψ_e is a function dependent on the total strain ε; the strain energy of the spring in Maxwell element, ψ_{ev}, is a function dependent on the elastic strain ε^{ev}; and the strain energy of the spring in the plastic branch, ψ_{ep}, is a function dependent on the elastic strain ε^{ep}.

For isothermal processes, the entropy inequality reduces to the following statement that the stress power minus the rate of change of free energy must be non-negative:

$$\sigma\dot{\varepsilon} - \dot{\psi} \geq 0 \tag{5}$$

and it can be further reduced to the following:

$$\frac{\partial \psi_{ev}}{\partial \varepsilon^{ev}}\dot{\varepsilon}^{v} + \frac{\partial \psi_{ep}}{\partial \varepsilon^{ep}}\dot{\varepsilon}^{p} \geq 0 \tag{6}$$

This inequality shows that the choices of the evolution equations for the inelastic strains ε^v and ε^p are not arbitrary if the model is required to be compatible with the dissipation inequality. This inequality can be satisfied in the sense of sufficient conditions by appropriate flow rules, as follows:

$$\dot{\varepsilon}^{v} = \frac{1}{\eta_v}\sigma^{v} \text{ and } \dot{\varepsilon}^{p} = \frac{1}{\eta_p}|\dot{\varepsilon}^{p}|\sigma^{p} \tag{7}$$

where, $\eta_v > 0$ is the viscosity and $\eta_p > 0$, is a material constant. Since the rate-dependent response is nonlinear and the relaxation behavior depends on the loading history, the viscosity should be a function of process quantities. Different flow rules can be used as long as they satisfy Eq. (6).

Internal variables based models: Stress convolution: The stress convolution models are based on an additive decomposition of the second Piola-Kirchhoff stress tensor, instead of the deformation gradient tensor, into equilibrium and nonequilibrium parts. The equilibrium response is assumed to be governed by a free energy function $\psi_{eq}(G)$; while the nonequilibrium response is characterized by a set of nonequilibrium free energy functions $\psi^k_{neq}(G)$, where k represents the kth relaxation mechanism of the material and each of them is associated with a nonequilibrium stress Q^k, Ref. 17. One or more relaxation mechanisms may be considered in the model. Note that both parts of the strain energy are functions of the total strain G, which is different from the deformation decomposition based models. The second Piola-Kirchhoff stress tensor, for a generalized Zener model, is given as

$$S(t) = S_{eq} + S_{neq} = 2\frac{\mathrm{d}\psi_{eq}(G)}{\mathrm{d}G} + \sum_{k=1}^{N} Q^k(t) \tag{8}$$

A simple linear evolution equation which governs the nonequilibrium stress is postulated as [Refs. 18-19],

$$\frac{\mathrm{d}}{\mathrm{d}t}Q^k(t) + \frac{1}{\tau^k}Q^k(t) = \frac{\mathrm{d}}{\mathrm{d}t}\left[2\frac{\mathrm{d}\psi^k_{neq}(G)}{\mathrm{d}G}\right] \tag{9}$$

$$Q^k(t)|_{t=0} = Q^k_0$$

where τ^k is the relaxation time related to the kth relaxation. Eq. (9) can be written in a *convolution* form as

$$Q^k(t) = Q^k_0 \exp(-\frac{t}{\tau^k}) + \int_{-\infty}^{t} \exp\left[-\frac{t-s}{\tau^k}\right]\frac{\mathrm{d}}{\mathrm{d}s}\left[2\frac{\mathrm{d}\psi^k_{neq}(G)}{\mathrm{d}G}\right]\mathrm{d}s \tag{10}$$

This model is well known to be computationally efficient; however, it has not been conclusively proven to satisfy the second law of thermodynamics for all admissible processes.

Haupt-Sedlan Model (H-S Model)

To easily and clearly understand the fundamental characteristics of the elastomeric material models, two models will be evaluated based on a simple shear deformation, as depicted in Fig. 8. The right part of the figure shows one elastomeric sample in its reference (solid line) and deformed (dashed line) configurations. The deformation is assumed as plane strain state and the ratio of the length to width is assumed to be >>1.

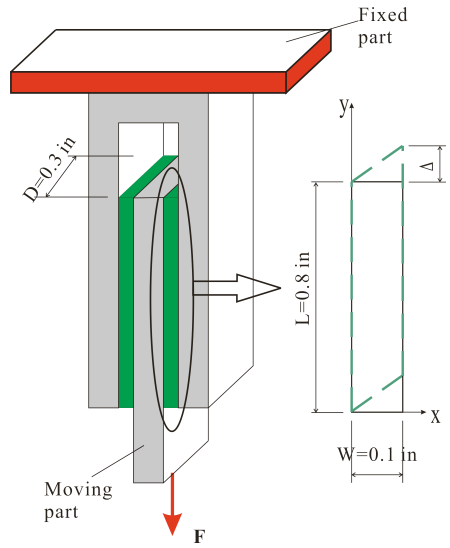

Fig. 8. Elastomer specimen under double-lap shear test.

For a material point with coordinates $\underline{x} = (x, y, z)$ in the reference configuration, its coordinates become $\underline{X} = (x, y + \gamma x, z)$ in the deformed configuration, where $\gamma = \Delta / W$ is the shear strain. The deformation gradient is as follows:

$$F = \frac{\mathrm{d}\underline{X}}{\mathrm{d}\underline{x}} = \begin{bmatrix} 1 & 0 & 0 \\ \gamma & 1 & 0 \\ 0 & 0 & 1 \end{bmatrix} \tag{11}$$

The right Cauchy-Green strain tensor is as follows:

$$G = F^T F \tag{12}$$

The invariants of the right Cauchy-Green strain tensor are defined as follows:

$$I_1 = \mathrm{tr}(G) = 3 + \gamma^2 \tag{13a}$$

$$I_2 = \frac{1}{2}\left[(\mathrm{tr}G)^2 - \mathrm{tr}(GG)\right] = 3 + \gamma^2 \tag{13b}$$

$$I_3 = \det(G) = 1 \tag{13c}$$

Since $I_3 = 1$, a volume preserving deformation is under consideration.

When a strain energy function ψ is assumed, the second Piola-Kirchhoff stress tensor can be derived from it as follows:

$$\sigma_{ij} = 2\frac{\partial \psi}{\partial G_{ij}} = 2\left(\frac{\partial \psi}{\partial I_1}\frac{\partial I_1}{\partial G_{ij}} + \frac{\partial \psi}{\partial I_2}\frac{\partial I_2}{\partial G_{ij}}\right) \tag{14}$$

Considering $\frac{\partial I_1}{\partial G_{ij}} = \delta_{ij}$ and $\frac{\partial I_2}{\partial G_{ij}} = I_1\delta_{ij} - G_{ij}$, the second Piola-Kirchhoff stress tensor can be computed as:

$$\sigma_{ij} = \begin{bmatrix} \sigma_{11} & \sigma_{12} & 0 \\ \sigma_{21} & \sigma_{22} & 0 \\ 0 & 0 & \sigma_{33} \end{bmatrix} \tag{15}$$

with

$$\sigma_{11} = 2\frac{\partial \psi}{\partial I_1} + 4\frac{\partial \psi}{\partial I_2} \tag{16a}$$

$$\sigma_{12} = \sigma_{21} = -2\gamma\frac{\partial \psi}{\partial I_2} \tag{16b}$$

$$\sigma_{22} = \sigma_{33} = \sigma_{11} - \gamma\sigma_{12} \tag{16c}$$

The second Piola-Kirchhoff stress tensor, Eq. (15), can be transformed to the Cauchy stress tensor as follows:

$$\tau_{ij} = F\sigma_{ij}F^T = \begin{bmatrix} \sigma_{11} & \gamma\sigma_{11} + \sigma_{12} & 0 \\ \gamma\sigma_{11} + \sigma_{21} & \gamma^2\sigma_{11} + \gamma(\sigma_{12} + \sigma_{21}) + \sigma_{22} & 0 \\ 0 & 0 & \sigma_{33} \end{bmatrix} \tag{17}$$

This Cauchy stress can be further decomposed into spherical and deviatoric parts, respectively, as

$$p = \frac{1}{3}(\tau_{11} + \tau_{22} + \tau_{33}) = \sigma_{11} + \frac{1}{3}\gamma^2\sigma_{11} \tag{18a}$$

$$\tau_{ij}^{\mathrm{dev}} = \tau_{ij} - p\delta_{ij}$$

$$= \begin{bmatrix} -\frac{\gamma^2}{3}\sigma_{11} & \gamma\sigma_{11} + \sigma_{12} & 0 \\ \gamma\sigma_{11} + \sigma_{21} & \frac{2\gamma^2}{3}\sigma_{11} + \gamma\sigma_{12} & 0 \\ 0 & 0 & -\frac{\gamma^2}{3}\sigma_{11} - \gamma\sigma_{12} \end{bmatrix} \tag{18b}$$

Note that the deviatoric stress components τ_{11}^{dev}, τ_{22}^{dev}, and τ_{33}^{dev} are higher order terms in terms of the shear strain γ compared with τ_{12}. Hence, when γ is assumed to be small, these components can be neglected. In the following discussions, only the shear strain γ and shear stress τ_{12} will be considered. In other words, this simple shearing deformation is considered as a one-dimensional problem. The subscript for the shear stress τ_{12} will be omitted in the following discussions.

The one-dimensional version of the Haupt-Sedlan model, the H-S model, Ref. 15, is shown in Fig. 9 below. It consists of elastic, viscous, and plastic branches in parallel. The total shear stress is written as

$$\tau = \tau_e + \sum_m \tau_p + \sum_n \tau_v \tag{19}$$

where τ_e, τ_p, and τ_v are the elastic equilibrium stress, hysteretic equilibrium stress and overstress contributions to the total response, and m and n are the number of plastic and viscous branches the model may include,

respectively. The total strain in the plastic and viscous branches is decomposed into the elastic and plastic parts, and elastic and viscous parts, respectively,

$$\gamma = \gamma_{ep} + \gamma_p \text{ and } \gamma = \gamma_{ev} + \gamma_v \tag{20}$$

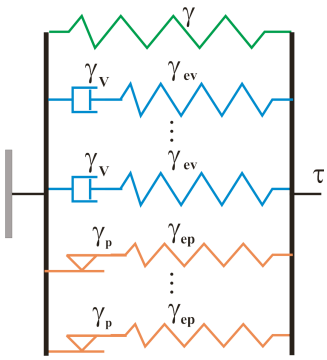

Fig. 9. One-dimensional rheological representation of H-S model.

The evolution laws governing the plastic and viscous strains are assumed as the following forms, respectively:

$$\dot{\gamma}_p = \frac{1}{\eta_p} |\dot{\gamma}| \tau_p \tag{21a}$$

$$\dot{\gamma}_v = \frac{1}{\eta_v} \tau_v \tag{21b}$$

where $\eta_v > 0$ is the viscosity and $\eta_p > 0$ a material constant. The viscosity is assumed as a function of process variables as follows:

$$\eta_v = \frac{c_v}{\xi |\dot{\gamma}| + 1/\tau_0} \tag{22}$$

where c_v and ξ are material constants. The relaxation time τ_0 is allowed to vary between a minimum τ_{min} and a maximum value τ_{max} according to:

$$\tau_0 = \tau_{max}(1-q) + \tau_{min} q \tag{23}$$

where q is structural variable governed by the following initial-value problem:

$$\dot{q} = \zeta |\dot{\gamma}| (1-q) - \frac{1}{\tau_q}\sqrt{q}, \; q(0) = 0 \tag{24}$$

where ζ and τ_q are additional material parameters. Note that q is between 0 and 1.

The elastic equilibrium stress τ_e, hysteretic equilibrium stress τ_p and overstress τ_v can be related to the shear strain γ, plastic strain γ_p, and viscous strain γ_v, respectively, using strain energy density functions. Currently, the strain energy functions corresponding to τ_e, τ_p and τ_v are assumed to take the following forms:

$$\begin{aligned}\psi_e &= c_1(I_1-3) + c_2(I_2-3) + c_3(I_1-3)(I_2-3) \\ &\quad + c_4(I_2-3)^2 + c_5(I_1-3)^3\end{aligned} \tag{25a}$$

$$\psi_{ep} = c_{p1}(I_{ep1}-3) + c_{p2}(I_{ep2}-3) \tag{25b}$$

$$\psi_{ev} = c_{v1}(I_{ev1}-3) \tag{25c}$$

where I_{ep1} and I_{ev1} are the first invariants of the right Cauchy-Green strain tensor corresponding to the deformation gradient tensor resulting from γ_{ep} and γ_{ev}, respectively. From these strain energy functions, the stress tensor can be computed. The elastic equilibrium shear stress is as follows:

$$\begin{aligned}\tau_e &= \tau_{12}^e = \gamma\sigma_{11}^e + \sigma_{12}^e \\ &= 2(c_1+c_2)\gamma + 4(c_3+c_4)\gamma^3 + 6c_5\gamma^5 \\ &\equiv c_{e1}\gamma + c_{e2}\gamma^3 + c_{e3}\gamma^5\end{aligned} \tag{26}$$

and the hysteretic equilibrium stress and overstress are as follows:

$$\tau_p = 2(c_{p1}+c_{p2})\gamma_{ep} \equiv c_p(\gamma - \gamma_p) \tag{27a}$$

$$\tau_v = 2c_{v1}\gamma_{ev} \equiv c_v(\gamma - \gamma_v) \tag{27b}$$

Eqs. (19) to (24) and (26) to (27) define the complete H-S elastomeric material model.

H-S elastomeric material model implementation

The material parameters required for the H-S model can be obtained as follows:

1) First, the elastic and plastic material parameters are identified from relaxation tests. The relaxation stress can be considered as the elastic and plastic response only when the time scale is sufficiently long for a relaxation test. The parameters involved in the elastic and plastic behavior of the material can be identified by fitting the elastic and plastic response of the H-S model to the measured relaxation data.
2) Second, the viscous material parameters are identified from relaxation and harmonic strain tests. Once the parameters involved in the elastic and plastic behavior of the material are identified, the elastic and plastic response can be computed and subtracted from the experimentally measured total stress history to get the overstress history from which the parameters involved in the viscous behavior of the material can be identified.

H-S model response under harmonic strain. In this section, some of the model parameters based on storage and loss moduli determined through a sinusoidal shear test are identified. In this case, a harmonic strain history is prescribed, as follows:

$$\gamma = A\sin(\omega t) \tag{28}$$

The corresponding steady state stress history would be as follows:

$$\tau = c_0 + c_1 \cos(\omega t) + d_1 \sin(\omega t) + c_2 \cos(2\omega t) + d_2 \sin(2\omega t) + \cdots \tag{29}$$

From these strain and stress histories, the storage modulus, G', and loss modulus, G'' are as follows:

$$G' = \frac{d_1}{A} \tag{30a}$$

$$G'' = \frac{c_1}{A} \tag{30b}$$

The above expressions can then be fitted to experimental data to identify the material parameters.

Since it is not easy to get a closed-form expression for the structural variable q (Eq. 24) when a harmonic strain is applied, in the following discussion, the relaxation time τ_0 is assumed to be constant and independent of q. After the harmonic behavior of the model with constant relaxation time is studied, the influence of q on the storage and loss moduli will be discussed.

Experimental-data fitting. Once the analytical formulations for the storage and loss moduli are determined, these expressions can be used to identify the unknown material parameters by fitting to test data. The identification procedure involves the minimization of the error between Eqs. (30) and the test data, with the following error function:

$$\|e\|^2 = (\underline{G}' - \underline{G}'_{exp})^T (\underline{G}' - \underline{G}'_{exp}) + (\underline{G}'' - \underline{G}''_{exp})^T (\underline{G}'' - \underline{G}''_{exp}) \tag{31}$$

where $\underline{G}'$ and $\underline{G}''$ are the analytical expressions, Eqs. (30), and $\underline{G}'_{exp}$ and $\underline{G}''_{exp}$ are the experimental test data.

The test data used for the fitting procedure was obtained from Ref. 20 and consists of the storage and loss moduli measured at the following strain amplitudes and frequencies:

$$A = \{0.02, 0.05, 0.10, 0.15\} \tag{32a}$$

$$f = \{1.0, 5.0, 10.0, 15.0, 20.0\} \text{ Hz} \tag{32b}$$

Figures 10-11 show the fitted storage and loss moduli together with the test data. It can be seen that the H-S material model with constant relaxation time is capable of fitting the storage modulus quite well while the same is not true for the loss modulus.

H-S model with non-constant relaxation time, harmonic response. In the previous section, the relaxation time was assumed to be constant and it has been shown that this model is not capable of predicting the loss modulus behavior. In this section, the model predictions are investigated with a variable structural parameter q. Numerical simulations have been performed with the identified material parameters from the fitting procedure for Figs. 10-11 together with assumed parameters involved in determining q.

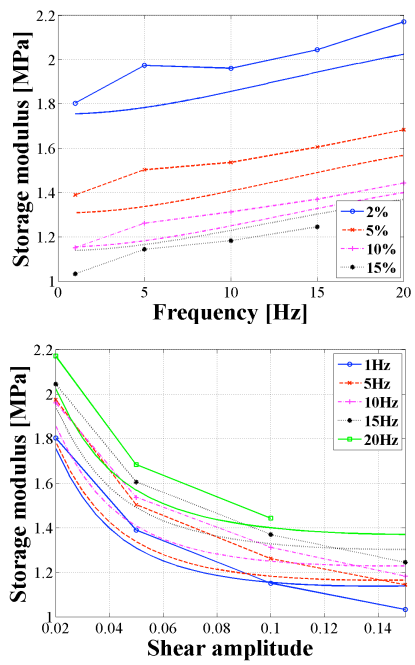

Fig. 10. Storage modulus fitting. With symbols: test data; without symbols, Eqs. (30).

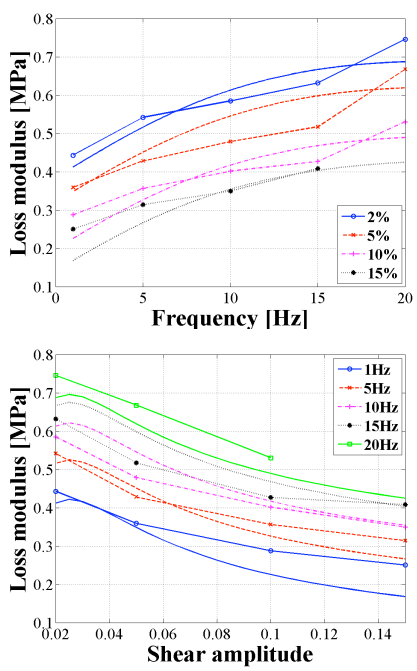

Fig. 11. Loss modulus fitting. With symbols: test data; without symbols, Eqs. (30).

The stress response of the material was computed with harmonic strain, Eq. (28), as input. A Fourier transformation was then performed on the stress history to get the components with same frequency as that of the input strain. Finally, the storage and loss moduli were calculated from Eqs. (30). The results are shown in Figs. 12-13. From these figures, it can be seen that the loss modulus is much better fitted. The model now captures the general form of the loss modulus variation with frequency and shear strain amplitude. It is believed that, if the material parameters were better tuned, the H-S model can give even better predictions.

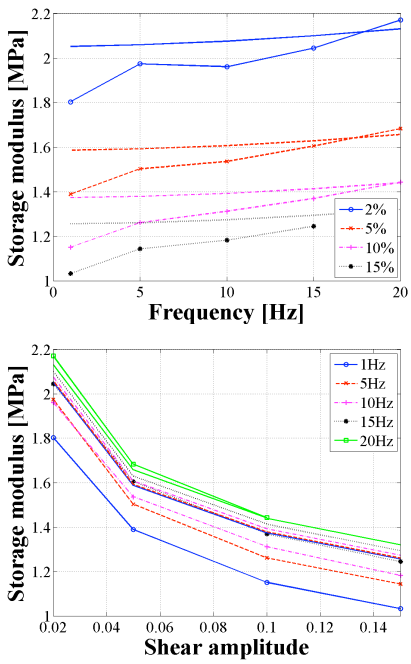

Fig. 12. Storage modulus with assumed q related parameters.

One important thing that should be pointed out is that the previous analysis and discussions are all based on the fact that the H-S model consists of one elastic, one plastic and one viscous path in parallel. However, as indicated in Eq. (19), the H-S model can involve several plastic and/or viscous paths in parallel. It can be expected that the predictions from H-S model will have a better agreement with the actual behavior of elastomeric materials when more plastic and/or viscous paths are included in the model. Figs. 14-15 present the storage and loss moduli fitting but this time with three viscous paths (or Maxwell elements). It can be seen that the fitted results are much better than those shown in Figs. 10-11 where only one Maxwell element was used.

H-S model response under relaxation test. Typical relaxation stress and relaxation moduli have been obtained and the trends agree with the experimental observations reported by Austrell [Ref. 20]. The results are not shown here. These results are similar to the ones discussed later using the Höfer-Lion model, shown in Fig. 22.

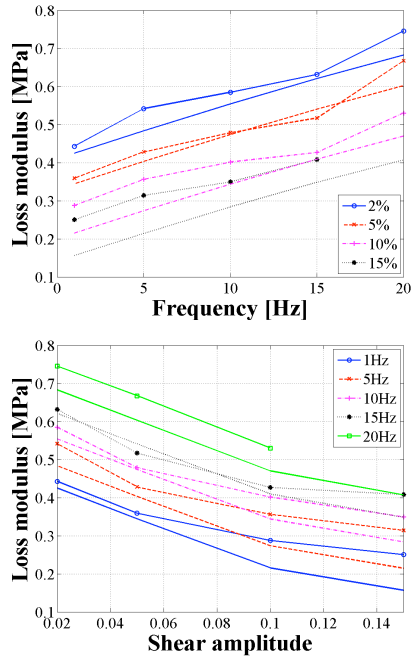

Fig. 13. Loss modulus with assumed q related parameters.

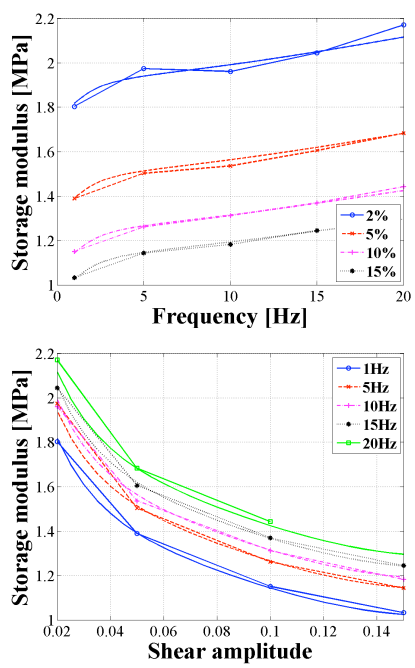

Fig. 14. Storage modulus fitting. With symbols: test data; without symbols, Eqs. (30) for case with three Maxwell elements.

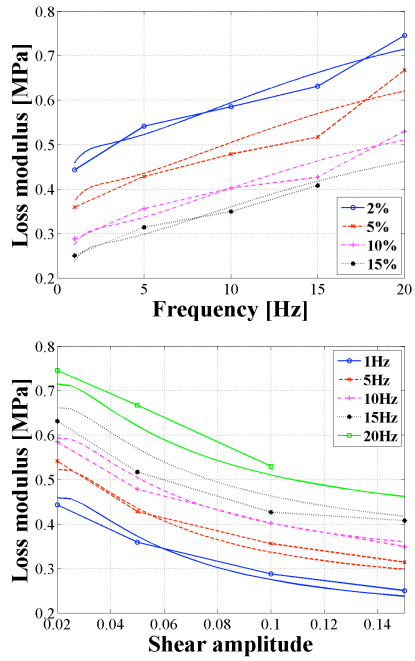

Fig. 15. Loss modulus fitting. With symbols: test data; without symbols, Eqs. (30) for case with three Maxwell elements.

Numerical simulations. Numerical simulations with the H-S model have been performed to evaluate its capability to capture the typical experimental observations for elastomers. Simulations have been performed with two specified strain histories that separately simulate a maneuver and a variable-thrust flight profile. In the first strain profile, the strain amplitude is increased and then decreased, Fig. 16, a maneuver flight profile. In the second strain profile, a static offset is introduced, Fig. 17, a variable-thrust flight profile.

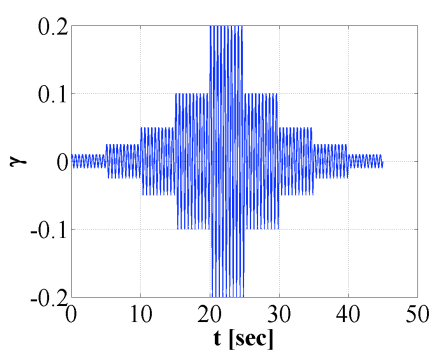

Fig. 16. Sinusoidal strain with increasing and decreasing amplitudes.

Results for the sinusoidal strain with increasing-decreasing amplitude, Fig. 16, showed that whether the strain amplitude is increasing or decreasing does not affect the storage and loss moduli of the material as long as the application time is long enough for each amplitude. This means that the decline in the modulus due to an increase of the strain amplitude is recoverable, which is in accordance with the experimental results reported in Ref. 20. Simulation on a sinusoidal strain with static offset, Fig. 17, showed that the strain offset has little influence on the loss modulus but affects the storage modulus if the stress-strain relationship for the elastic response is nonlinear.

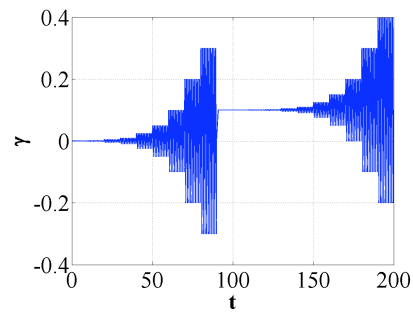

Fig. 17. Sinusoidal strain with static strain offset.

Overall, the above studies are encouraging regarding the suitability of the H-S model for predicting the behavior of typical elastomeric materials. The H-S model includes all the necessary elements - elastic, plastic, and viscous - to model a carbon filled elastomer. However, to be able to fully judge the performance of the model, experimental data for the actual damper material is required. Elastomers are complex materials and an analytical model that works for one specific type of material may not work for all elastomer types.

Höfer-Lion Model (H-L Model)

The Höfer and Lion model, H-L model, Ref. 21, is a recent, time domain formulation for finite nonlinear viscoelasticity with distinct relaxation and recovery behavior of the storage and loss moduli, and the authors claim that their modeling approach can predict the recovery behavior of typical elastomers quite well. The H-L elastomeric material model has been currently evaluated in this study by comparing its predictions with the sample experimental data provided by SKF. Finally, responses of the H-L model to typical strain profiles have been investigated.

H-L model constitutive equations

The H-L model is based on the concept of stress decomposition. The one-dimensional version consists of one elastic path and one or more Maxwell elements in parallel. The total shear stress can be additively decomposed as follows:

$$\tau = \tau_e + \sum_{m=1}^{M} \tau_{vm} \tag{33}$$

where τ_e is the elastic equilibrium shear stress which can be given by any physically meaningful stress-strain relationship, for example:

$$\tau_e = c_e \gamma \tag{34}$$

In Eq. (33), τ_{vm} is the over-stress in the *m*th Maxwell element, given by:

$$\dot{\tau}_{vm} = c_{vm}\dot{\gamma} - \frac{\dot{z}_m}{\tau_{0m}}\tau_{vm} \quad \text{for } m = 1, 2, \ldots, M \tag{35}$$

Here z_m is an intrinsic time scale and τ_{0m} the relaxation time. Note that if $z_m = t$, Eq. (35) becomes the equation for the standard linear Maxwell element with viscosity $\eta_{vm} = c_{vm}\tau_{0m}$, which is well-suited for modeling the frequency-dependent properties of elastomeric materials but cannot describe any amplitude-dependent phenomena. To model both the amplitude- and frequency-dependent behaviors of elastomeric materials, the evolution of z_m is given by the following differential equation:

$$\dot{z}_m(t) = \alpha_m\left(\bar{\tau}_m |\dot{\gamma}| + 1\right) + \left(1 - \alpha_m\right)\left(\sum_{i=1}^{L} d_{mi} q_i + 1\right) \quad \text{for } m = 1, 2, \ldots, M \tag{36}$$

Here α_m, $\bar{\tau}_m$ and d_{mi} are material parameters and q_i are the internal variables to describe the amplitude dependence of the material. q_i are given by a set of first order differential equations in the following form:

$$\dot{q}_i(t) = \frac{1}{\tau_{qi}}\left(\tau_{q0}|\dot{\gamma}| - q_i\right) \quad \text{for } i = 1, 2, \ldots, L \tag{37}$$

The parameters τ_{qi} are relaxation times describing the dynamic behavior of the material's microstructure and the constant $\tau_{q0} = 1$ sec is introduced for dimensional reasons.

The two terms on the right-hand side of Eq. (36) were proposed for different purposes. The first term describes the short-term behavior of the material between amplitude steps, while the second term is included to describe the long-term recovery behavior of the modulus. The characteristics of these two terms are discussed as follows. When $\alpha = 1$, the H-L model consists of only the first term, and the model will be referred to as the *α -1 model*; when $\alpha = 0$, the H-L model consists of only the second term, and will be referred to as the *α -0 model*.

α -1 model. For the α -1 model, Eq. (35) becomes (with the subscript *m* omitted):

$$\dot{\tau}_v = c_v\dot{\gamma} - \frac{\bar{\tau}|\dot{\gamma}| + 1}{\tau_0}\tau_v \tag{38}$$

This is the differential equation for a Maxwell element with relaxation time, as follows:

$$\tau_R = \frac{\tau_0}{\bar{\tau}|\dot{\gamma}| + 1} \tag{39}$$

Accordingly, the viscosity for the Maxwell element is:

$$\eta_v = c_v\tau_R = \frac{c_v}{\xi|\dot{\gamma}| + 1/\tau_0} \tag{40}$$

with $\xi = \bar{\tau}/\tau_0$. Note that this viscosity is the same as the expression for the viscosity of Haupt-Sedlan model (Eq. (22) in the H-S Model section) which means that the α -1 model is the same as the H-S model but with a constant τ_0. Hence, the behavior of the α -1 model will not be discussed here. Earlier discussions on the H-S model with constant τ_0 apply to the α -1 model as well.

α -0 model. For the α -0 model, Eq. (35) becomes:

$$\dot{\tau}_v = c_v\dot{\gamma} - \frac{\sum_{i=1}^{L} d_i q_i + 1}{\tau_0}\tau_v \tag{41}$$

with evolution equations given by Eq. (37) for *q*. The behavior of this α -0 model is, in general, different from the α -1 model. However, considering the case where *q* achieves a steady state (constant), $\dot{q} = 0$, then $q = \tau_{q0}|\dot{\gamma}|$. Then Eq. (41) becomes:

$$\dot{\tau}_v = c_v\dot{\gamma} - \frac{\tau_{q0}\left(\sum_{i=1}^{L} d_i\right)|\dot{\gamma}| + 1}{\tau_0}\tau_v \tag{42}$$

The α -0 model in this case is the same as the α -1 model with $\bar{\tau} = \tau_{q0}\left(\sum_{i=1}^{L} d_i\right)$, Eq. (38).

H-L material model implementation

H-L model response under harmonic strain. Earlier, the H-S model with constant τ_0 was fitted to the experimental storage and loss moduli. In this section, the same fitting procedure is applied to the α -1 and α -0 models to study their capability to model the amplitude- and frequency-dependency of the elastomeric materials. Figs. 18-19 below present the storage and loss moduli fits for the α -1 and α -0 models with one Maxwell element in parallel, while Figs. 20-21 show the results for the α -1 and α -0 models with three Maxwell elements in parallel.

Note that the test data used here was obtained for "an" elastomeric material that is not necessarily the formulation used for damper applications. Some key observations from these two sets of figures, Figs. 18-21, are as follows:

1) The overall fit for the storage modulus is better than that for the loss modulus.

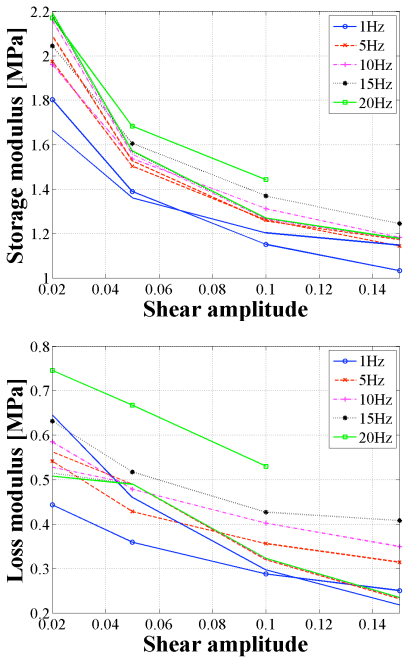

Fig. 18. Storage and loss moduli fitting vs. shear amplitude. With symbols: test data; without symbols: α -1 model fitting with one Maxwell element.

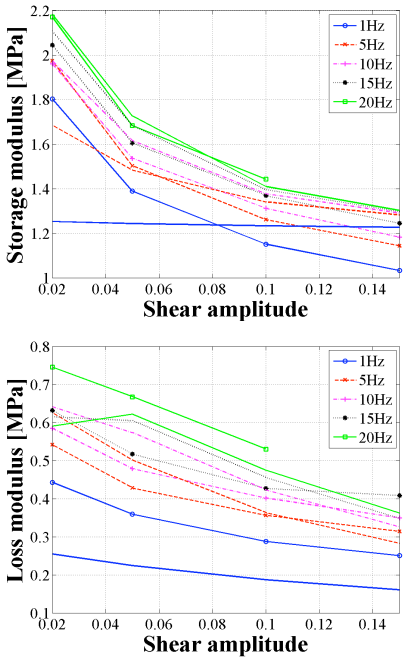

Fig. 19. Storage and loss moduli fitting vs. shear amplitude. With symbols: test data; without symbols: α -0 model fitting with one Maxwell element.

2) The α -1 model performs better than α -0 model for the storage modulus fitting, while the α -0 model works better than α -1 model for the loss modulus fitting.

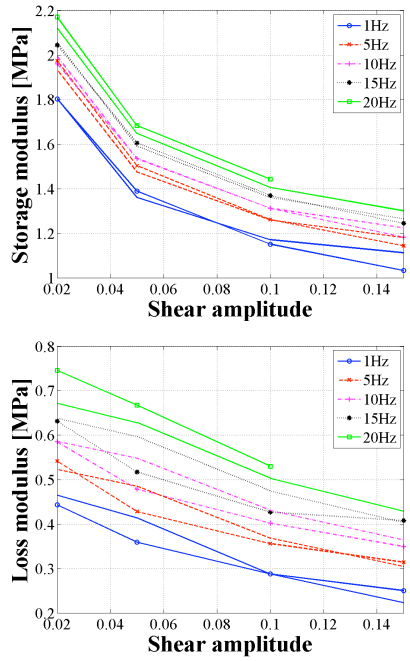

Fig. 20. Storage and loss moduli fitting vs. shear amplitude. With symbols: test data; without symbols: α -1 model fitting with three Maxwell elements.

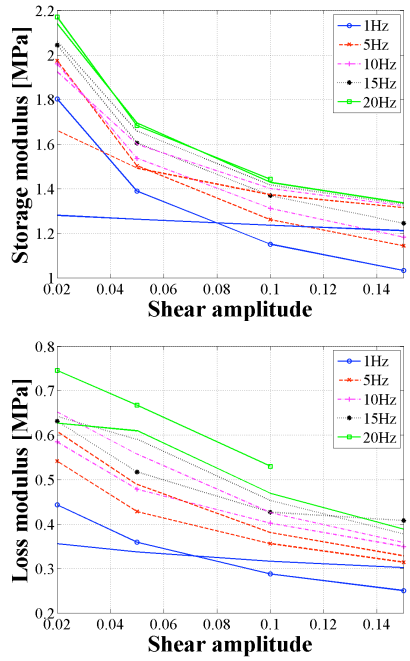

Fig. 21. Storage and loss moduli fitting vs. shear amplitude. With symbols: test data; without symbols: α -0 model fitting with three Maxwell elements.

3) The fit for the α-1 model becomes much better when the number of parallel Maxwell elements increases whereas similar fitting improvement with the increasing number of parallel Maxwell elements is not apparent for the α-0 model.

H-L model response under relaxation test. Typical relaxation stress and relaxation moduli are shown in Fig. 22 below. In the top figure, a larger stress corresponds to a larger strain, as expected. In the bottom figure, however, a larger relaxation modulus corresponds to a smaller strain step size, i.e. the relaxation modulus decreases with increasing strain step size. These results agree with the experimental observations reported in Ref. 20.

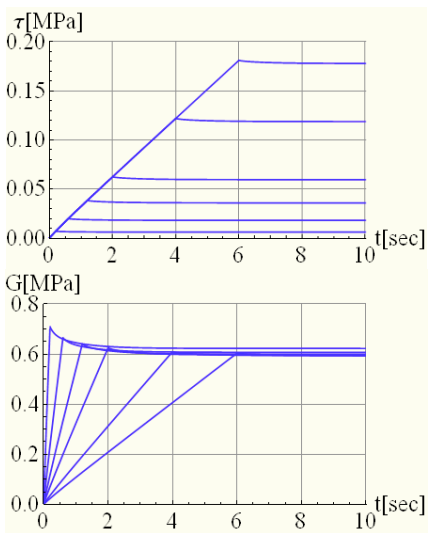

Fig. 22. Relaxation vs. time. Top: relaxation stress; bottom: relaxation modulus.

Numerical simulations. Numerical simulations were performed with the two special strain histories, Figs. 16-17. Results for a sinusoidal strain with increasing-decreasing amplitude, Fig. 16, showed that whether the strain amplitude is increasing or decreasing does not affect the storage and loss moduli of the material as long as the application time is long enough for each amplitude. This means that the decline in the modulus due to an increase of the strain amplitude is recoverable, which is in accordance with the experimental results reported in Ref. 20. However, if the application time of the strain is not long enough compared with the material recovery time, the moduli between increasing and decreasing amplitude sequences are different. The significance of this difference depends on the relative length of the strain application time to the material recovery time.

Simulation on a sinusoidal strain with static offset, Fig. 17, showed that the effect of the static strain offset on both the storage and loss moduli is negligible for the offsets investigated.

Overall, the above studies are encouraging regarding the suitability of the H-L model for predicting the behavior of typical elastomeric materials. Compared with the H-S model, the H-L model does not have a plastic element, and also, the stress-strain relationship for the elastic response is linear. However, these drawbacks can be overcome by including one or more plastic elements in the H-L model, and replacing the stress-strain relationship for the elastic response with a nonlinear relationship, which should improve the performance of the H-L model. As noted earlier, however, to be able to fully judge the performance of the models, the experimental data for the actual damper material is required. Elastomers are complex materials and an analytical model that is good for one specific type of material may not be good for all elastomer types.

H-L model evaluation summary

From the preceding analytical studies, the following conclusions, similar to those for the H-S model, can be drawn for the H-L model as follows:

1) The H-L model is capable of capturing the frequency and the amplitude dependency of the storage and loss moduli.
2) Predictions from the H-L model under relaxation tests agree with the typical experimental observations for elastomeric materials under relaxation tests.
3) Simulation results for a sinusoidal strain with increasing and then decreasing amplitude showed that whether the strain amplitude is increasing or decreasing does not affect the storage and loss moduli of the material as long as the settling time is long enough for each amplitude. However, if the settling time is not long enough compared to the recovery time, the modulus for the same amplitude in increasing and decreasing sequences is different.
4) The static strain offset does not affect the storage and loss moduli.

The material parameters identification procedure for this H-L model would be easier than that for the Haupt-Sedlan model since closed-form expressions for the stress history of the H-L model under harmonic strain or relaxation test can be obtained. These expressions can then be fitted to the experimental data to identify the material parameters.

Comparison of H-S and H-L models

Two elastomeric material models, the Haupt-Sedlan and the Höfer-Lion models, have been thoroughly analyzed in this study. These analyses were based on a simple shear

deformation case, a deformation state close to the actual work state of the lead-lag dampers used in rotorcraft. From our studies, it has been found that both the H-S and the H-L models are capable of predicting some typical experimental observations for elastomeric materials, and the overall predictions from these two models are quite similar.

The H-S model includes the necessary elements for modeling elastomeric materials: the elastic, plastic, and the viscous element. Hence, in theory, the H-S model should be able to model the behavior of the elastomeric materials if the material parameters are well-tuned. However, the equation governing the structural variable q, Eq. (24), is difficult to solve analytically, even for a very simple strain history.

Also, the H-L model does not have a plastic element and the stress-strain relationship for the elastic response is linear. However, this drawback can be overcome by including one or more plastic elements in the H-L model and replacing the stress-strain relationship for the elastic response with a nonlinear relationship, which should improve the performance of the H-L model.

Material Characterization Testing

Our repeated efforts to find a suitable source that could provide the relevant constitutive material property data that could be used in the current effort were unsuccessful. Consequently, the required material characterization tests will be performed by MTC/Georgia Tech to obtain the desired constitutive property data. In this respect, the Aerospace Division of SKF Corporation is expected to furnish samples, nominally $152.4\ \text{mm} \times 152.4\ \text{mm} \times 2.54\ \text{mm}$, of the production elastomeric material used in its damper installed in the new Bell M429 helicopter. MTC/Georgia Tech have initiated the design of a new experimental test setup for the material characterization tests. This task involves building a new mechanical test system and performing material characterization tests to generate the desired property data.

Concluding Remarks

An analytical, first-principles modeling study on helicopter elastomeric dampers was presented. The goal of this ongoing study is to model the critical behaviors that rotorcraft elastomeric dampers exhibit, i.e. the hyperelastic, viscous, and nonlinear behaviors involving hysteresis loops. First-principles models predict the behavior of a device based on a continuum mechanics approach in which the geometric configuration of the various components of the device is modeled using, for example, a finite element approach, and the material behavior is represented by an appropriate set of nonlinear constitutive laws. On completion of the present effort, the current model would not require the damper to exist *a priori*. The model and the methodology therein could be used to optimize the design of a damper concept.

Sample results were presented. An initial, overall validation effort has demonstrated the successful step-by-step sample development of a new finite element damper model and, importantly, its integration with the multibody dynamics analysis DYMORE. Two material models, the Haupt-Sedlan model and the recently proposed Höfer-Lion model, have been analyzed, and the results have been fitted to sample experimental data. Both models gave acceptable results for the storage and loss moduli. Since at present there is a dearth of available appropriate material data for the typical elastomers used in helicopter dampers, a new experimental effort has been initiated by Materials Technologies Corporation (MTC) and Georgia Tech to conduct materials testing and acquire the required material data.

Acknowledgements

This ongoing Phase II SBIR study is funded by the NASA Subsonic Rotary Wing Project. Further details may be requested from Dr. Sesi Kottapalli, NASA Ames.

References

1. Flugge, W., “Viscoelasticity.” 2nd edition. 1975, Springer-Verlag.

2. Felker, F.F., Lau, B.H., McLaughlin, S., and Johnson, W., “Nonlinear behavior of an elastomeric lag damper undergoing dual-frequency motion and its effect on rotor dynamics.” *Journal of the American Helicopter Society*, 32(4), 1987 pp. 45-53.

3. Gandhi, F. and Chopra, I., “Analysis of bearingless main rotor aeroelasticity using an improved time domain nonlinear elastomeric damper model.” *Journal of the American Helicopter Society*, 41(3), 1996 pp. 267-277.

4. Lesieutre, G.A., “Finite elements for modeling frequency-dependent material damping using internal state variables.” 1992. Baltimore, MD, USA: Publ by ASTM, Philadelphia, PA, USA.

5. Lesieutre, G.A., Bianchini, E. and Maiani, A., “Finite element modeling of one-dimensional viscoelastic structures using anelastic displacement fields". *Journal of Guidance, Control, and Dynamics*, 19(3), 1996 pp. 520-527.

6. Smith, E.C., Govindswamy, K., Beale, M.R. and Lesieutre, G.A., “Formulation, validation, and application of a finite element model for elastomeric lag dampers.”

Journal of the American Helicopter Society, 41(3), 1996 pp. 247-256.

7. Smith, E.C., Govindswamy, K., Beale, M.R., Vascsinec, M.J. and Lesieutre, G.A., "Aeroelastic response and stability of helicopters with elastomeric lag dampers." *Journal of the American Helicopter Society*, 41(3), 1996 pp. 257-266.

8. Brackbill, C.R., Smith, E.C. and Lesieutre, G.A., "Application of a refined time domain elastomeric damper model to helicopter rotor aeroelastic response and stability." *Journal of the American Helicopter Society*, 47(3), 2002, pp. 186-197.

9. Kunz, D.L., "On the characterization of elastomeric materials for modeling helicopter lag damper." 1997. Kissimmee, FL, USA: AIAA, New York, NY, USA.

10. Miehe, C. and Keck, J., "Superimposed finite elastic-viscoelastic-plastoelastic stress response with damage in filled rubbery polymers. Experiments, modelling and algorithmic implementation." *Journal of the Mechanics and Physics of Solids*, 48(2), 2000 pp. 323-365.

11. Austrell, P.E., Olsson, A.K. and Jonsson, M., "A method to analyze the non-linear dynamic behaviour of carbon-black-filled rubber components using standard finite element code." Proceedings of the Second European Conference on Constitutive Models for Rubber, Germany, 2001.

12. Bauchau, O.A., Bottasso, C.L., and Nikishkov, Y.G., "Modeling rotorcraft dynamics with finite element multibody procedures." *Mathematics and Computer Modeling*, 33, 1113-1137, 2001.

13. Mullins, L. and Tobin, N.R., "Stress softening in rubber vulcanizates. Part I: Use of a strain amplification factor to describe the elastic behavior of filler-reinforced vulcanized rubber." *Journal of Applied Polymer Science*, 9, 1965 pp. 2993–3009.

14. Harwood, J.A.C., Mullins, L., and Payne, A.R., "Strees softening in natural rubber vulcanizates. Part II: Stress softening effects in pure gum and filler loaded rubbers." *Journal of Applied Polymer Science*, 9, 1965 pp. 3011–3021.

15. Haupt, P. and Sedlan, K., "Viscoplasticity of elastomeric materials: experimental facts and constitutive modeling." *Archive of Applied Mechanics*, 71, 2001 pp. 89-109.

16. Lion, A., "A physically based method to represent the thermo-mechanical behavior of elastomers." *Acta Mechanica*, 123, 1997 pp. 1-25.

17. Govindjee, S. and Reese, S., "A presentation and comparison of two large deformation viscoelasticity models." *Journal of Engineering Materiais and Technology*, 119, 1997 pp. 251-255.

18. Simo, J. C., "On a fully three-dimensional finite-strain viscoelastic damage model: Formulation and computational aspects." *Computer Methods in Applied Mechanics and Engineering*, 60, 1987 pp. 153-173.

19. Holzapfel, G.A., "On large strain viscoelasticity: continuum formulation and finite element applications to elastomeric structure." *International Journal for Numerical Methods in Engineering*, 39, 1996 pp. 3903-3926.

20. Austrell, P.E., *Modeling of Elasticity and Damping for Filled Elastomers*. PhD thesis, Lund Institute of Technology, Division of Structural Mechanics, Lund, Sweden, 1993.

21. Höfer, P. and Lion, A., "Modeling of frequency- and amplitude-dependent material properties of filler-reinforced rubber." *Journal of the Mechanics and Physics of Solids*, 57, 2009 pp. 500–520.